Astron. Astrophys. 340, 103–116 (1998)

ASTRONOMY AND ASTROPHYSICS

Radiative transfer in the clumpy environment of young stellar objects

S. Wolf[1], **O. Fischer**[2], **and W. Pfau**[2]

[1] Thüringer Landessternwarte Tautenburg, Sternwarte 5, D-07778 Tautenburg, Germany
[2] Astrophysikalisches Institut und Universitäts-Sternwarte, Schillergässchen 2, D-07745 Jena, Germany

Received 8 May 1998 / Accepted 27 July 1998

Abstract. We developed a Monte-Carlo code for the treatment of the radiative transfer in arbitrary clumpy dust configurations. Both the radiation of the (central) energy source(s) and the thermal emission of the dust are considered. Intensity and polarization maps of the modelled objects can be computed.

As the first application of our code we studied the radiative transfer in a spherical two-phase clumpy dust shell containing a single star. The structure of the circumstellar dust density distribution is characterized by the filling factor of high-density clumps, the density ratio between the low and the high density phases and the size of the smallest individual clumps.

Firstly, we considered the properties of the clumpy structures of that model using the percolation theory. Particularly, we checked different ways to describe the optical depth. Secondly, we investigated the total stellar flux, the mean scattering number and the absorption of the stellar radiation depending on the filling factor, the density ratio, the optical depth, the dust grain size and the smallest clump size. Thirdly, we compared the polarizing influence of a clumpy and an homogeneous dust shell. Fourthly, we investigated the influence of a clumpy density structure on the surface brightness distribution.

First results show significant changes in the spectral energy distribution as well as in images of clumpy dust configurations in comparison to their homogeneous counterparts.

Key words: radiative transfer – methods: numerical – methods: statistical – reflection nebulae – ISM: structure

1. Introduction

During the last 20 years many models for the description of the physical and chemical structure of interstellar clouds and circumstellar shells have been developed. Many of them assume homogeneous density distributions, although the density structures are obviously clumpy. The clumpy structure of the ISM, ranging over a large scale of sizes (e.g., see Colomb et al. 1980, Herbstmeier et al. 1993, Meyer & Blades 1995, Rosen & Bregman 1995, Spyromilio et al. 1995, Chen et al. 1996), can be observed both in our and in other galaxies (e.g., see Rohlfs & Luks 1992, Macchetto et al. 1994, Capetti et al. 1995a, 1995b, 1995c, Frisch 1996, Young 1996, Kishimoto 1998). For circumstellar dust shells a number of indications for their clumpy structure exist (e.g., see Lagrange et al. 1987, Burton et al. 1990, Falgarone et al. 1991, Stacey 1993, Mitskevich 1994, 1995, Matsamura & Seki 1995, Grinin et al. 1994, 1995, 1996). In consequence of these observations, the principal question for the difference in the data interpretation on the basis of homogeneous and clumpy media came up. Former attempts of the treatment of the radiative transfer in clumpy media were mostly done for 2-phase clumpy media using the Monte-Carlo or the Markov method (e.g. see Boissé, 1990; Meixner & Tielens 1993, 1995; Hobson & Scheuer 1993; Hobson & Padman 1993; Spaans 1996; Witt & Gordon 1996). The clumpy structure has been modelled using either spherical clumps or fractal-like density distributions defined on two or three-dimensional grids.

It was our intention to describe and apply the radiative transfer in clumpy dust shells around young stellar objects. After the introduction of our model (Sect. 2) we present in Sect. 3 the results of our investigations of the flux outside the shell, the mean scattering number, and the absorption of the stellar radiation in dependence on the different model parameters. In detail, these parameters are the filling factor and the density ratio (3.1.2), the optical depth (3.1.3), and the smallest clump size (3.1.4). Furthermore, we investigate the influence of clumpiness on the polarization state of the stellar light (3.2) and the visual surface brightness distribution(3.3).

2. The model

The model consists of a point-like star situated in the centre of a spherical dust shell with radius $R_{\rm s}$. The dust density distribution is defined on a three-dimensional cartesian grid with $N_{\rm x} \times N_{\rm y} \times N_{\rm z}$ grid points which are the centres of cubes with the size $l_{\rm c}$ ($l_{\rm c}$ is the distance between two neighbouring grid points). The diameter of a spherical dust shell with $N_{\rm s}$ grid points along each coordinate axis is $(N_s + 1) * l_{\rm c}$. The density at a certain grid point represents the density in the whole cube. A 2-phase clumpy medium with an uniform clump distribution can be created by assigning every grid point either to a low ($n_{\rm min}$) or a high ($n_{\rm max}$) dust number density in a stochastic way. The innermost region around the star is free of dust. Cubes with a common face and the

Send offprint requests to: S. Wolf, (wolf@tls-tautenburg.de)

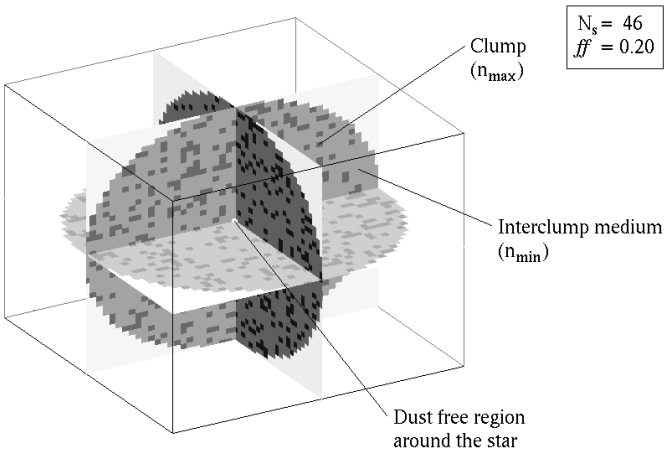

Fig. 1. Spherical circumstellar dust shell with a 2-phase clumpy dust distribution.

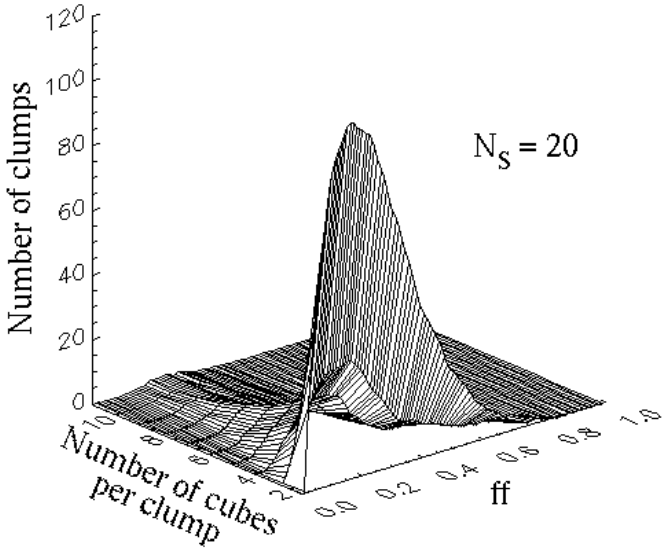

Fig. 2. Clump size spectrum of a spherical dust shell after 100 runs of the filling procedure.

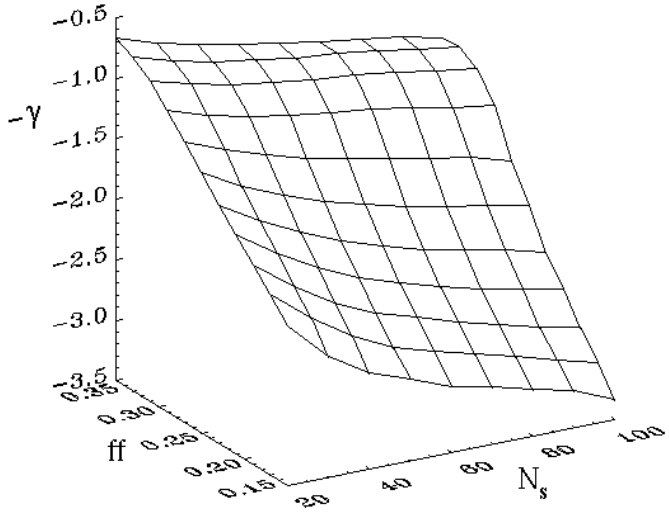

Fig. 3. Critical exponent $\gamma(N_{\rm S}, ff)$

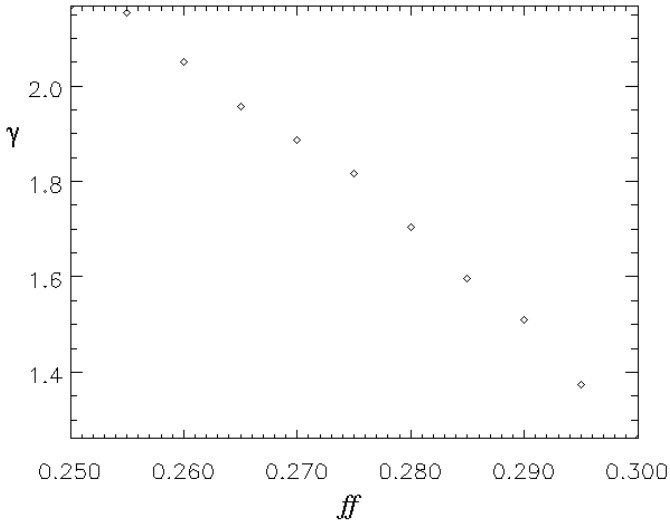

Fig. 4. Critical exponent $\gamma(N_{\rm S} = 100, ff)$ near the percolation threshold

same density belong to the same clump (also called cluster). The clumpy structure is characterized by the filling factor ff (ratio of the number of high density cubes to all cubes), the density ratio k between the low and high density phases, and the length scale of the smallest individual clump $l_{\rm c}$. With a constant mean value of the dust number density $\bar{n}$, $n_{\rm min}$ and $n_{\rm max}$ are only functions of the filling factor ff and the density ratio k:

$$n_{\rm max}(ff,k) = \frac{\bar{n}}{(1-ff)k+ff}, \quad (1)$$

$$n_{\rm min}(ff,k) = kn_{\rm max}. \quad (2)$$

Because of the stochastic way to fill the cubes, different runs of the filling procedure with the same parameters result in clumpy shells with different high density cube positions. To find out the mean properties of clumpy systems in respect to their radiation transfer it is therefore necessary to simulate a large number of dust shells, characterized by the same parameter set.

2.1. Percolation theory

The smallest scale on which clumps are produced by real clumping processes is much smaller than the entire volume in which such processes take place. This assumption is supported by observations of the clumpy structure of the interstellar medium in spiral and irregular galaxies (Colomb et al. 1980, Rosen & Bregman 1995) and by HST observations of the dust density distribution in the central regions of the galaxies NGC 1068 and Mrk 3 (Macchetto et al. 1994; Capetti et al. 1995 a,b,c). Limited by the computer storage we could only handle grids with up to 150^3 grid points. To check whether this resolution is high enough to simulate real clumpy structures, we made use of the percolation theory which gives the qualitative and quantitative description of cluster formation and related problems. For the check we determined the clump size spectrum for our models (see Fig. 2). The number of clumps with a volume smaller then 5% of the volume of the entire dust shell peaks

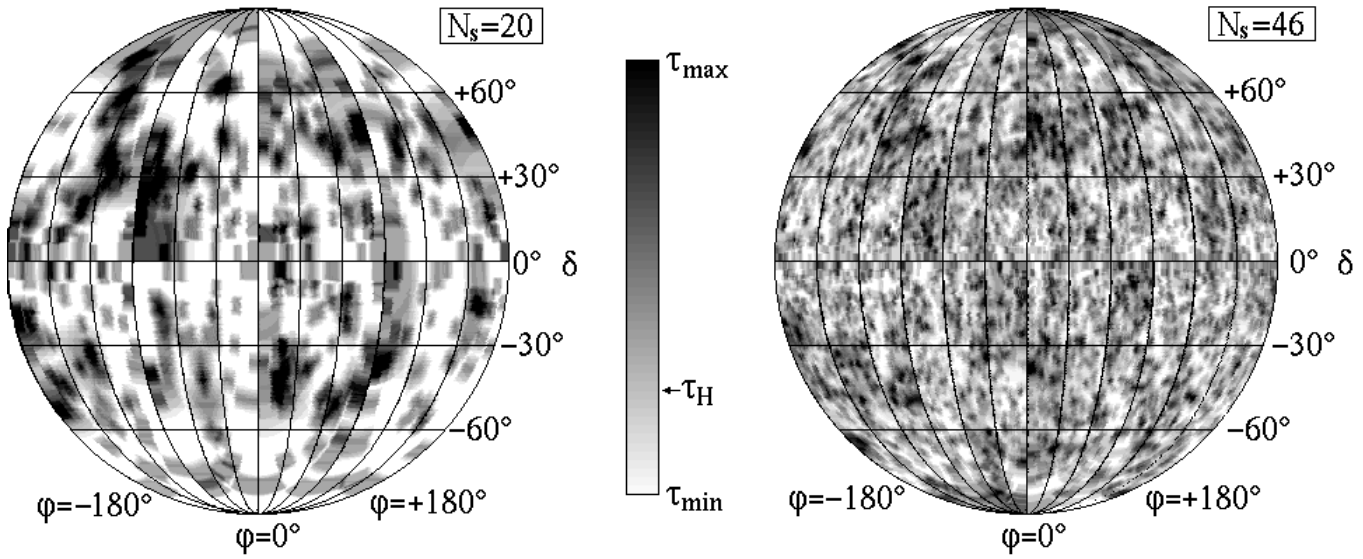

Fig. 5. Full solid angle representation of the distribution of the optical depth of the clumpy dust shell, seen from the star for two different grid sizes ($N_{\rm S}$=20 and $N_{\rm S}$=46), ff=0.10, k=0.01. The optical depth of the equivalent homogeneous shell $\tau_{\rm H}$ is the same for both shells. $\tau_{\rm min}, \tau_{\rm max}$ are the minimum and maximum optical depth; ϕ, δ are the spherical coordinates for each line of sight

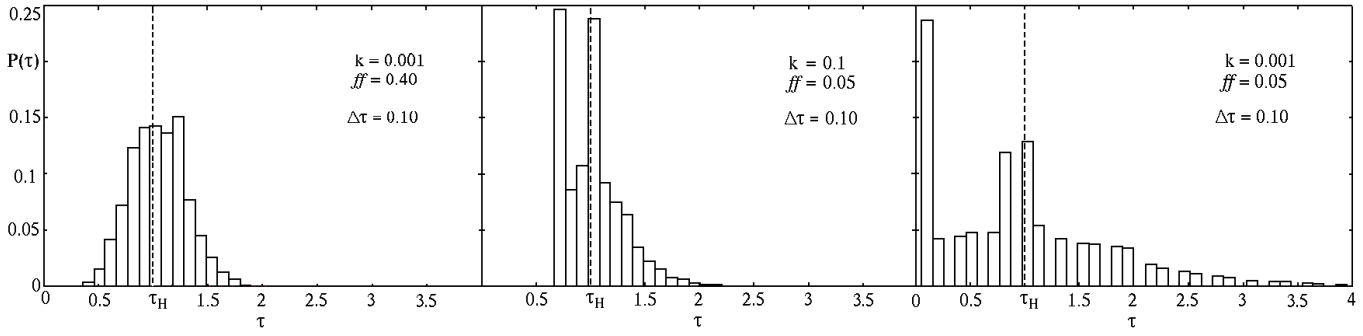

Fig. 6. The distribution of the optical depth P(τ)

in the range of $ff = 0.15 \ldots 0.20$. At higher filling factors ($ff \geq 0.70$) there are predominantly single clumps. The grid, on which the density distribution is defined, is characterized by its percolation threshold $ff_{\rm PT}$. This is the smallest filling factor at which at least one clump extends through the whole system with infinite grid points. The percolation threshold of our grid type is $ff_{\rm PT} \approx 0.246$ (see Stauffer et al. 1995). The percolation theory gives a potential law (3) for the clump size spectrum near the percolation threshold, where $K(s)$ is the number of clumps consisting of s grid points, and γ is the so-called critical exponent:

$$K(s) \propto s^{-\gamma}. \tag{3}$$

In Fig. 3 the critical exponent is shown for the filling factors $ff = (ff_{\rm PT} - 0.1) \ldots (ff_{\rm PT} + 0.1)$ and different grid sizes. For each grid size $N_{\rm S}$ and filling factor ff, 100 clumpy dust spheres were randomly created and the clump size spectrum was determined. For the individual dust spheres the critical exponent γ_i ($i = 1 \ldots 100$) was calculated through linear regression using Eq. 3. From this we got $\gamma(N, ff)$ as the arithmetic mean value of all $\gamma_i(N, ff)$. In the range near the percolation threshold, γ increases with increasing grid size. For dust shells with a diameter of $N_S = 100$ grid points, the difference to the critical exponent of an endless grid $\gamma(N_{\rm S} = \infty, ff_{\rm PT}) = 2.18$ is already lower than 0.5%.

Because of the constant density of the modelled clumps ($n_{\rm max}$), the mass spectrum is equivalent to the clump size spectrum. In diffuse interstellar clouds (DICs) and giant molecular clouds (GMCs) the mass spectrum follows the potential law in Eq. 3. The exponent γ is about 2 in DICs and about 1.6 in GMCs (see Dickey & Garwood 1989). For the assumption of two-phase structurized clouds and size-independend clump density this leads to filling factors of $ff_{\rm DIC} \approx 0.26$ and $ff_{\rm GMC} \approx 0.28$ (see Fig. 4).

2.2. The description of the optical depth

Fig. 5 shows the distribution of the optical depth for 10^6 lines of sight along different radii (ff=0.10, k=0.01; $N_{\rm S}$=20 and $N_{\rm S}$=46). Using the larger grid ($N_{\rm S} = 46$) the distribution is

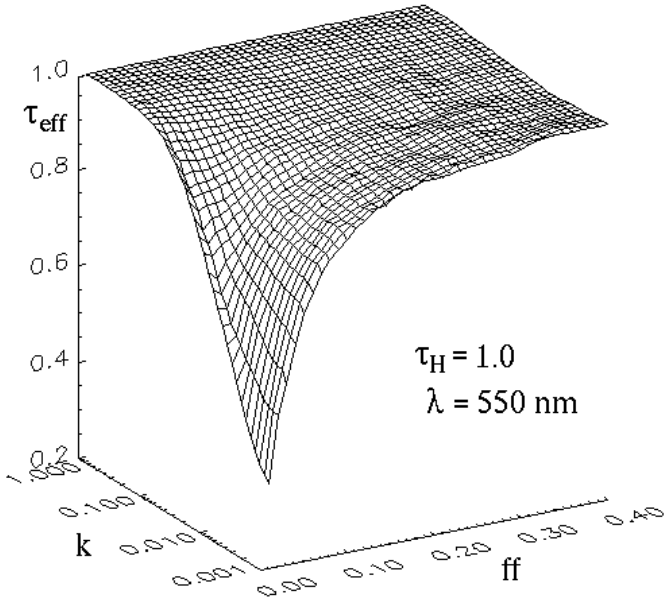

Fig. 7. $\tau_{\rm eff}(\tau_{\rm H}=1)$. λ = 550 nm. Population G (see text)

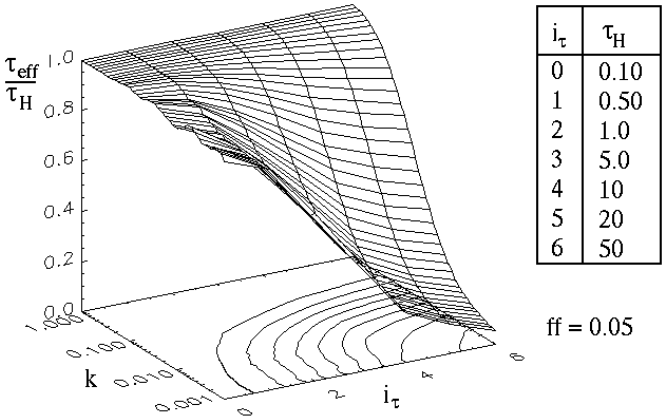

i_τ	$\tau_{\rm H}$
0	0.10
1	0.50
2	1.0
3	5.0
4	10
5	20
6	50

Fig. 8. Decreasing effective optical depth, normalized to the mean optical depth $\bar{\tau} \equiv \tau_{\rm H}$, depending on the density ratio. λ = 550 nm. Population G (see text)

much finer structured. The following investigations were done using a sphere with $N_{\rm S}$=46.

A quantitative description of the optical depth of clumpy systems can be done either in form of the the distribution of the optical depth P(τ) or by the effective optical depth $\tau_{\rm eff}$. For the comparison of both homogeneous and clumpy shells the optical depth of the equivalent homogeneous shell $\tau_{\rm H}$ is useful. The equivalent homogeneous shell is a dust shell with the same mass but with a constant density.

In this paper $\tau_{\rm eff}$ and $\tau_{\rm H}$ are calculated for $\lambda = 550$ nm.

2.2.1. The distribution of the optical depth

Fig. 6 shows the distribution of the optical depth $P(\tau)$ for different filling factors and density ratios for $\tau_{\rm H} = 1$ ($P(\tau)$ is the probability, that the optical depth along an arbitrary chosen

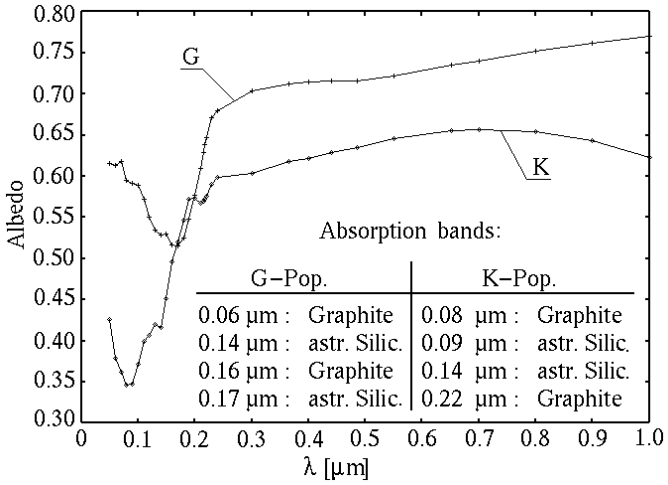

Fig. 9. Albedo of the G and K-population. The dots mark the wavelengths at which the radiation transfer was simulated.

line of sight has a value in the range $[\tau - \frac{\Delta\tau}{2}, \tau + \frac{\Delta\tau}{2})$). The shape of the distribution is not dependent on $\tau_{\rm H}$ and thus only a function of ff and k. Decreasing ff and/or k, it broadens both to lower and to higher optical depths. Below the percolation threshold a local maximum at $\tau_{\rm min} \approx \int_0^{R_s} C_{\rm ext} n_{\rm min} dr$ is added, where $C_{\rm ext}$ is the extinction cross section of the dust grains. It is caused by those lines of sight which lie only in dust with the density $n_{\rm min}$. For $ff \geq ff_{\rm PT}$ the number of those lines of sight is insignificant (or is equal to zero), but it is increasing for $ff < ff_{\rm PT}$. When decreasing k, then $n_{\rm min}$ and $\tau_{\rm min}$ also decrease.

2.2.2. Effective optical depth

Usually, clumpy envelopes have distributions of different optical depths. The effective optical depth $\tau_{\rm eff}$ gives us the possibility to describe the optical behaviour of clumpy envelopes by one parameter. It is defined as

$$\frac{S_{\rm g}(\lambda)}{S_*(\lambda)} = e^{-\tau_{\rm eff}(\lambda)}, \tag{4}$$

$$S_{\rm g} = \frac{S_*}{4\pi} \int_0^{2\pi} \int_0^{\pi} e^{-\tau(\theta,\phi)} \sin\theta d\theta d\phi \tag{5}$$

where $S_{\rm g}$ is the attenuated, non-scattered stellar flux integrated over all solid angle directions, and S_* is the original stellar flux at the wavelength λ (Witt & Gordon 1996). For $\tau_{\rm H} = 1$, $\tau_{\rm eff}$ was calculated using Eq. (6)

$$\tau_{\rm eff} = \lim_{n_{\rm M}\to\infty} \frac{1}{n_{\rm M}} \sum_{j=1}^{n_{\rm M}} \left[-\ln \left(\lim_{n_{\rm SL}\to\infty} \frac{1}{n_{\rm SL}} \sum_{i=1}^{n_{\rm SL}} e^{-\tau_i(\theta_i,\phi_i)} \right) \right] \tag{6}$$

where $n_{\rm M}$ is the number of models, and $n_{\rm SL}$ is the number of all chosen lines of sight uniformly distributed over 4π $ster$ (see Fig. 7).

For $\tau_{\rm H} = 1$ the effective optical depth rapidly decreases for $k < 0.1$ if $ff < ff_{\rm PT}$ (Fig. 7). While the radiative transfer

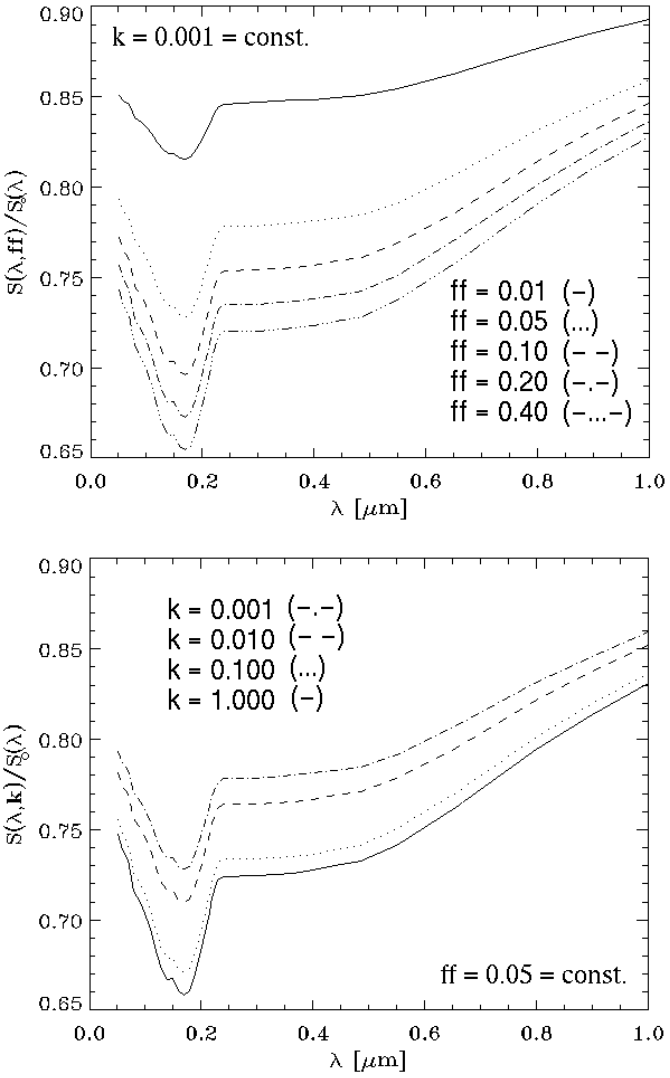

Fig. 10. Increase of the integrated stellar flux outside the dust shell following a decrease of either the k or ff. Population G, $\tau_{\rm H} = 1$

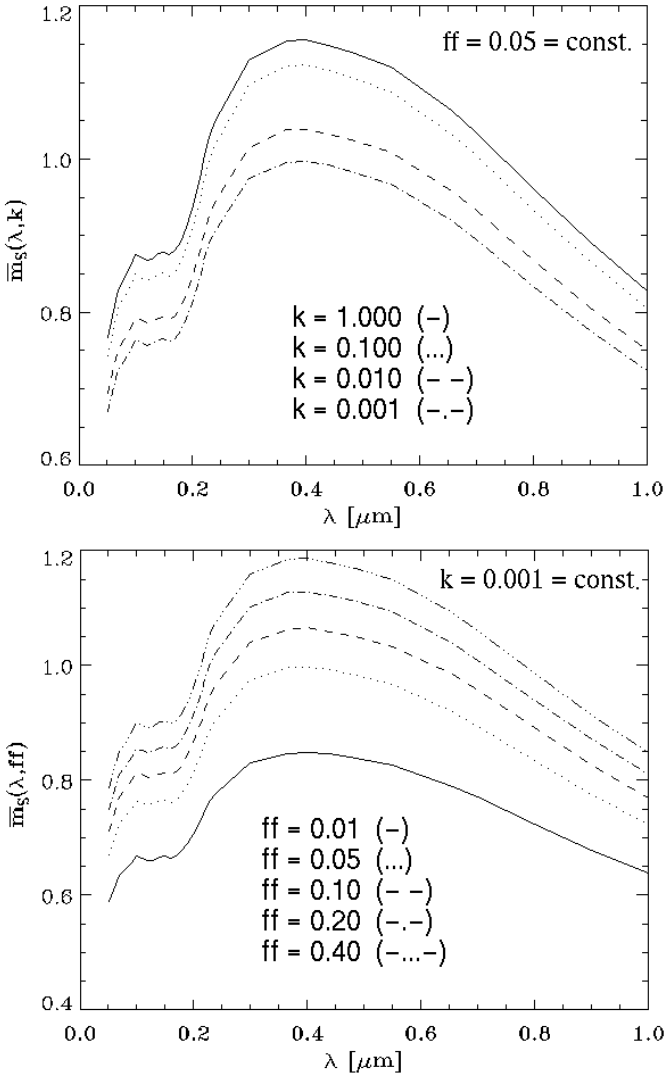

Fig. 11. Dependence of the mean scattering number $\bar{m}_{\rm s}$ of the test-photons on k and ff. Population G, $\tau_{\rm H} = 1$

above this value can be treated like in homogeneous media, for lower values of ff, respectively k, the dust shell appears essentially more transparent. These results are in agreement with those of Witt & Gordon (1996) and the numerical and analytical results of Boissé (1990) and Hobson & Scheuer (1993). The increase of $\tau_{\rm H}$ shifts these limits of ff and k to higher values (see Fig. 8).

2.3. The simulation of the radiative transfer

2.3.1. The program

For the simulation of the radiative transfer we developed a Monte-Carlo radiative transfer code. It is based on the code of Fischer et al. (1994) which was developed for the simulation of polarization maps of pre-main sequence objects. The radiation has been partitioned into so-called weighted test-photons. Every test-photon is characterised by its wavelength and its Stokes vector $(I, Q, U, V)_{\rm T}$ which becomes modified due to scattering and absorption.

Whereas the dust number density and the temperature distribution are defined on the 3-dimensional grid, the test-photon transfer is not coupled with this grid. In the case of a 2-phase clumpy but statistically homogeneous medium we chose a cartesian grid with equidistant grid points. The stellar radiation is modelled separately from the dust reemission which was not considered. This is possible because the stellar radiation peaks in the ultraviolet (UV) or the visible wavelength range (pre-main sequence stars, e.g., T Tauri) whereas the dust reemission of the absorbed energy of the star radiation occurs in the infrared (IR).

2.3.2. The dust

Calculations were performed with two different grain populations - a diffuse ISM-population ("K", radii between 0.005 and 0.25 μm) and a population with only larger grains ("G", radii

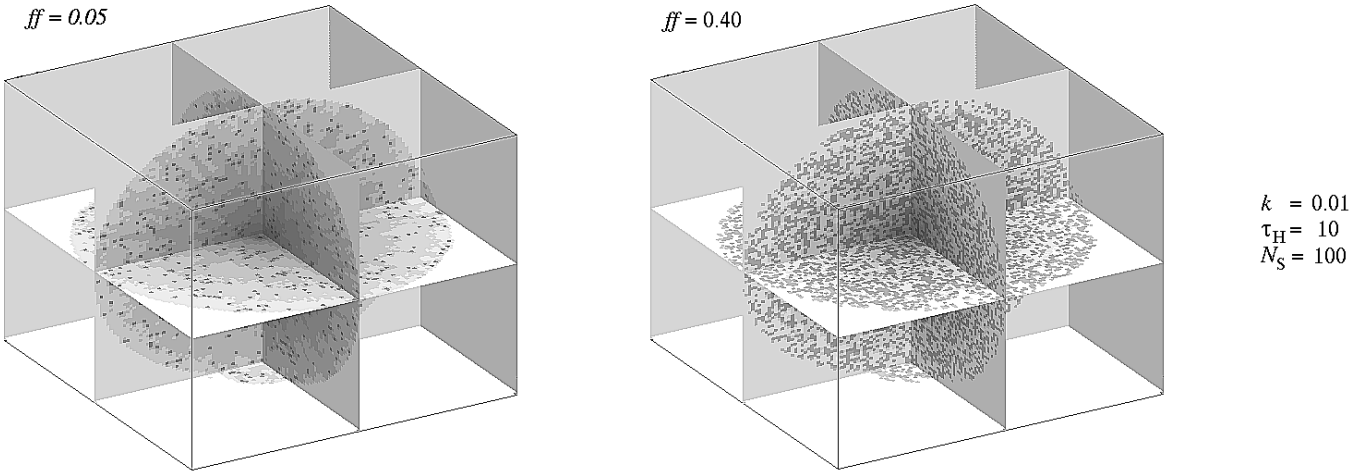

Fig. 12. Spatial representation of the regions of absorption. Dark/bright regions symbolize a strong/weak absorption. The darkest regions are identical with clumps.

between 0.1 and 1 μm). We used the optical data of Draine & Lee (1984). For both populations the grains are distributed with a number density $n(a) \propto a^{-3.5}$ (a is the radius of the spherical dust grains). We used a dust mixture of 62.5% "astronomical" silicate and 37.5% graphite (25% - **E** oscillates parallel to the graphite plane, 12.5% - **E** oscillates perpendicular to the graphite plane) as the basis for the optical dust data. The albedo for both dust populations G and K is shown for 0.050 μm $\leq \lambda \leq 1.000$ μm in Fig. 9.

As grains with different radii or of different materials have various cross sections ($C_{\rm sca}$, $C_{\rm ext}$) and elements of the scattering matrix, these grain parameters are expressed for a mixture in form of the corresponding "representative" values $< C_{\rm sca} >$, $< C_{\rm ext} >$, and $< \hat{S} >$:

$$< C_{\rm sca} >= \sum_{i=1}^{w} \int_{a_{\rm min}}^{a_{\rm max}} g_i(a) C_{{\rm sca}_i}(a) da, \quad (7)$$

$$< C_{\rm ext} >= \sum_{i=1}^{w} \int_{a_{\rm min}}^{a_{\rm max}} g_i(a) C_{{\rm ext}_i}(a) da, \quad (8)$$

$$< \hat{S} >= \sum_{i=1}^{w} \int_{a_{\rm min}}^{a_{\rm max}} g_i(a) \hat{S}_i(a) da \quad (9)$$

With regard to the optical effect of each component of the dust mixture, the weight $g_i(a)$ depends on the abundance of the i-th material component (w components are present) and on the size distribution of the dust particles (in the range between the smallest $a_{\rm s}^{(i)}$ and the largest $a_{\rm l}^{(i)}$ radii) of each component. Here, we have normalized $g_i(a)$ so that

$$\sum_{i=1}^{w} \int_{a_{\rm min}}^{a_{\rm max}} g_i(a) da = 1 \quad (10)$$

The "representative" value of the albedo can be calculated as follows:

$$< albedo >= \frac{C_{\rm sca}}{C_{\rm ext}} \quad (11)$$

3. Results

3.1. Stellar radiation through a clumpy dust shell

3.1.1. The simulation

The first application of our code concerned the investigation of the stellar flux through a clumpy dust envelope. We performed the radiative transfer for test-photons with wavelengths in the range 0.050 μm $\leq \lambda \leq 1.000$ μm. The transfer was simulated separately for 33 discrete wavelengths λ_i in this range. For every wavelength λ_i, N_i test-photons with the intensity $I = 1$ were started from the central star, symbolizing the stellar flux $S_{\rm o}(\lambda_i)$. The total intensity of all photons leaving the dust shell after absorption and scattering symbolizes the flux $S(\lambda_i, ff, k)$.

3.1.2. The influence of filling factor and density ratio

The ratio $\frac{S(\lambda,ff,k)}{S_0(\lambda)}$ increases, if k or ff decreases (Fig. 10). This behaviour results from the large probability $P(\tau)$ for test-photons to propagate along small optical depths, which appear in $P(\tau)$ for low filling factors and low density ratios. The shape of the curves in Fig. 10 originates from the absorption behaviour of the dust.

The mean scattering number $\bar{m}_{\rm s}$ defines the mean number of scatterings of a large sample of test-photons in a given dust shell. In contrast to the flux, it decreases, if the density ratio k or the filling factor ff decreases (see Fig. 11).

All of these results are consistent with the numerical results presented by Witt & Gordon (1996). The stellar light is scattered in the clumps more effectively than in the surrounding interclump medium. Contrary to this, the scattering probability decreases in the optical thin phase. In Fig. 12 this is demonstrated for k=0.01 and ff=0.05 or 0.40. Meridional planes through the clumpy spherical dust shell give a spatial representation of the regions of absorption (dark areas). For both cases the highest absorption rate is in the clumps (dark grey spots). The absorption by the interclump medium concentrates to the centre of the

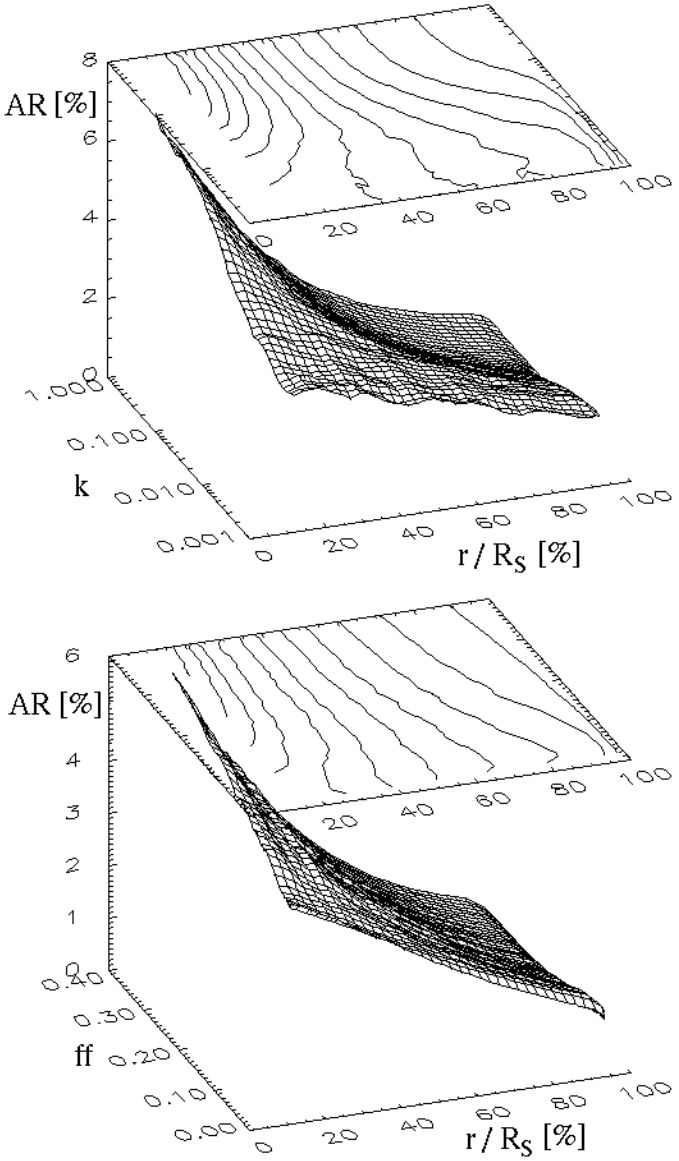

Fig. 13. Radial rate of absorption in the interclump medium. variation of either ff or k, $\tau_{\rm H} = 10$, Population G
Increasing the clumpiness (by decreasing k and/or ff)

- $\Rightarrow$ Decrease of the absorption in the inner region of the shell ($r/R_{\rm s} < 40\%$)
- $\Rightarrow$ Decrease of the absorption in the outer region of the shell ($r/R_{\rm s} \geq 40\%$)
- $\Longrightarrow$ Decrease of the gradient of the radial rate of absorption
- $\Longrightarrow$ Decrease of the gradient of the temperature in the interclump medium

envelope. We define the radial rate of absorption $AR(\rho)$ by

$$AR(\rho) = \frac{\frac{p_{\rm abs}(\rho)}{ff'(\rho)\rho^2}}{\int_0^{R_{\rm S}} \frac{p_{\rm abs}(\rho)}{ff'(\rho)\rho^2} d\rho} \qquad (12)$$

where $p_{\rm abs}$ is the percentage of all photons being absorbed in the shell of a sphere (radius ρ; thickness $d\rho$) in reference to all started photons and $ff'(\rho)$ is the filling factor of the shell. If the filling factor is low, the probability for photons to be scattered (and absorbed) more distant from the star is higher and, therefore, the gradient of the radial rate of absorption is smaller.

This correlation is shown by the representations of the radial rate of absorption in Fig. 13.

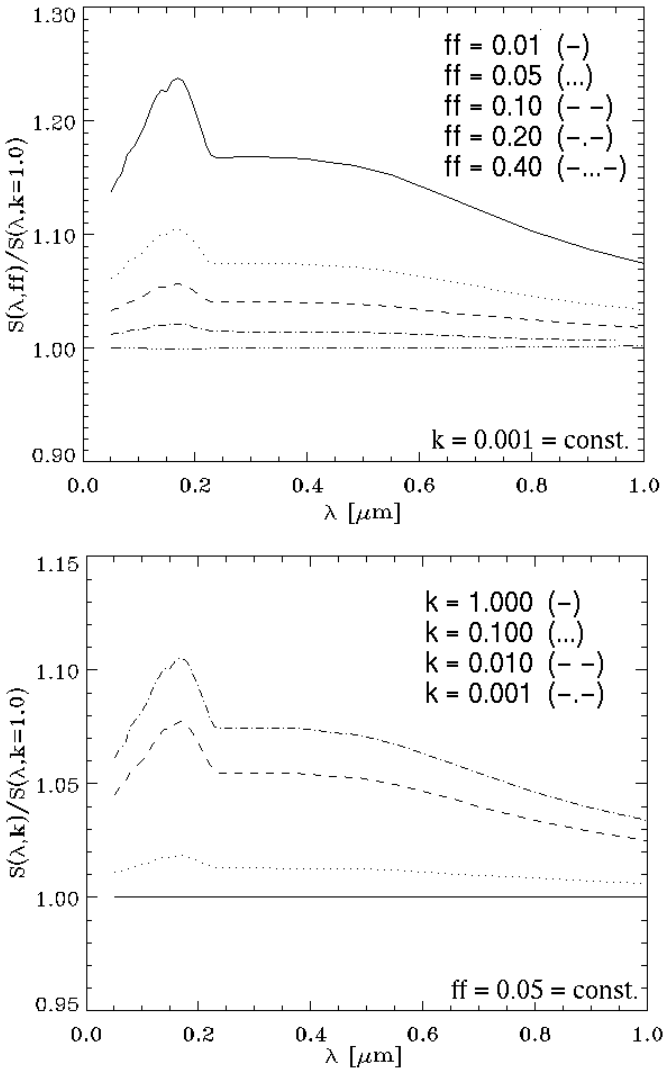

Fig. 14. Integrated stellar flux outside the clumpy dust shell $S(\lambda, ff)$. $\tau_{\rm H} = 1$. Population G

3.1.3. Influence of the optical depth

In Fig. 14 and 15 the ratio $\frac{S(\lambda,ff,k)}{S(\lambda,k=1)}$, where $S(\lambda, k = 1)$ is the stellar flux outside the equivalent homogeneous shell, is shown in dependence on the filling factor ff and the density ratio k for $\tau_{\rm H} = 1$ and $\tau_{\rm H} = 10$. Compared with the equivalent homogeneous shell clumpiness on the line of sight overemphasizes spectral features. For $\lambda \leq 0.2$ μm the ratio $\frac{S(\lambda,ff,k)}{S(\lambda,k=1)}$ behaves nearly in inverse proportion to the albedo of the dust. It increases with decreasing filling factor and density ratio and with increasing optical depth $\tau_{\rm H}$. This means that the absorption bands - described by the albedo of the dust - become weaker. If the

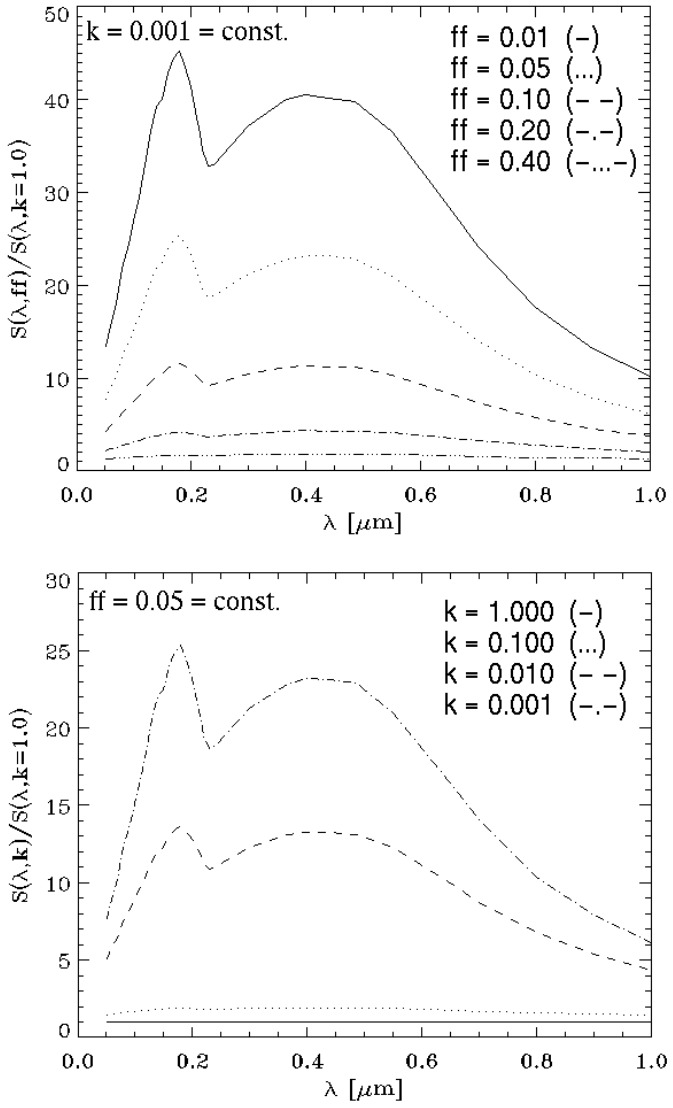

Fig. 15. Integrated stellar flux outside the clumpy dust shell $S(\lambda, ff)$. $\tau_{\rm H} = 10$. Population G

optical depth of the clumps is sufficiently high and that of the interclump medium is sufficiently low, the short wavelength radiation is modified by nearly grey extinction. Compared with an homogeneous shell of the same mass, the stellar light is less reddened. This effect was first discovered by Natta & Panagia (1984) on the basis of a much more simplified model. It can be explained by the covering effect of the clumps, which dominates at the conditions described above (see also Meixner & Tielens 1993, 1995). The stellar radiation reaches the observer after a small number of interactions mainly with the interclump dust particles and is thus less reddened. Radiation being scattered in the optical thick clumps leaves the circumstellar dust configuration strongly attenuated.

Since the qualitative behaviour of $\frac{S(\lambda,ff,k)}{S(\lambda,k=1)}$ depends only slightly on the wavelength, this ratio and the mean number of scatterings was determined only for $\lambda = 550$ nm in dependence on the values of $\tau_{\rm H}$, ff, and k (see Fig. 16). The higher $\tau_{\rm H}$ the stronger the clumpiness modifies the observable stellar radiation. According to the law of Lambert and Beer, the probability for a photon to leave the dust shell decreases exponentially with increasing optical depth. As a consequence, the interclump medium becomes of importance at increasing optical depth. Clumpiness becomes insignificantly for the radiative transfer for a low density contrast between the two phases.

As the results of Witt & Gordon (1996), our simulations also demonstrate that $\tau_{\rm H}$ is an important parameter for the characterization of clumpy dust shells. The ratio $\frac{S(\lambda,ff,k)}{S(\lambda,k=1)}$ is increased by more than one order of magnitude for $\tau_{\rm H} = 10$ due to the variation of ff and k (λ = 550 nm, see Figs. 14, 15).

Direct stellar fluxes, which differ strongly from those in the equivalent homogeneous shell can only be found for $k < 0.01$ and $ff < 0.2$. This is shown by radiative transfer runs which were performed for different values of ff and k. Starting with an homogeneous sphere it is not enough to decrease k to increase the flux, because the scattering probability is too large in a clumpy medium with $ff > ff_{\rm PT} \approx 0.25$. Below the percolation threshold ($ff < ff_{\rm PT}$), the stellar flux differs only insignificantly from that through the equivalent homogeneous shell for a density ratio nearly to 1 since the shell then resembles an homogeneous one.

The strong changes of the stellar flux in dependence on $\tau_{\rm H}$ result from a strong increase of the number density of the interclump medium for low filling factors and density ratios (see Sect. 2.2.2).

3.1.4. Influence of the smallest clump size

Whereas the previous calculations were done using grids with 46^3 grid points, the behaviour of the relative fluxes and mean scattering numbers for different grid sizes is shown in Fig. 17. The smallest cube size represents the size of the smallest clump; e.g. for $N_{\rm S}$=46, the smallest clump extension amounts to 2.2% of the shell diameter.

By the decrease of the relative clump size, the high density phase of dust is finer distributed in the shell. As a consequence, the photon scattering probability increases and the stellar flux outside the shell decreases. With the convergence of the smallest clump size to the mean distance between the dust particles of the dense phase, both dust density phases change into another - the statistically homogeneous dust distribution turns into that of an homogenous shell ($n_{\rm max}, n_{\rm min} \rightarrow \bar{n}$). Increasing the wavelength of the test-photons, the difference of the stellar fluxes, evaluated for different smallest clump sizes, decreases.

In our calculations we did not interpolate the density distribution between single grid points. Thus, the shape of the dust shell may differ noticeable from an exact sphere and the questions has to be answered, to what extent the results differ from reality. We found, that $\frac{S(\lambda,l_{\rm c})}{S_0(\lambda,l_{\rm c})}$ decreases, if the grid is enlarged. However, the differences between the relative stellar fluxes $\frac{S(\lambda,l_{\rm c})}{S_0(\lambda,l_{\rm c})}$ simulated for different grid sizes are smaller then about the factor 15 compared with the differences shown in Fig. 17. Thus, there is no significant influence on the found

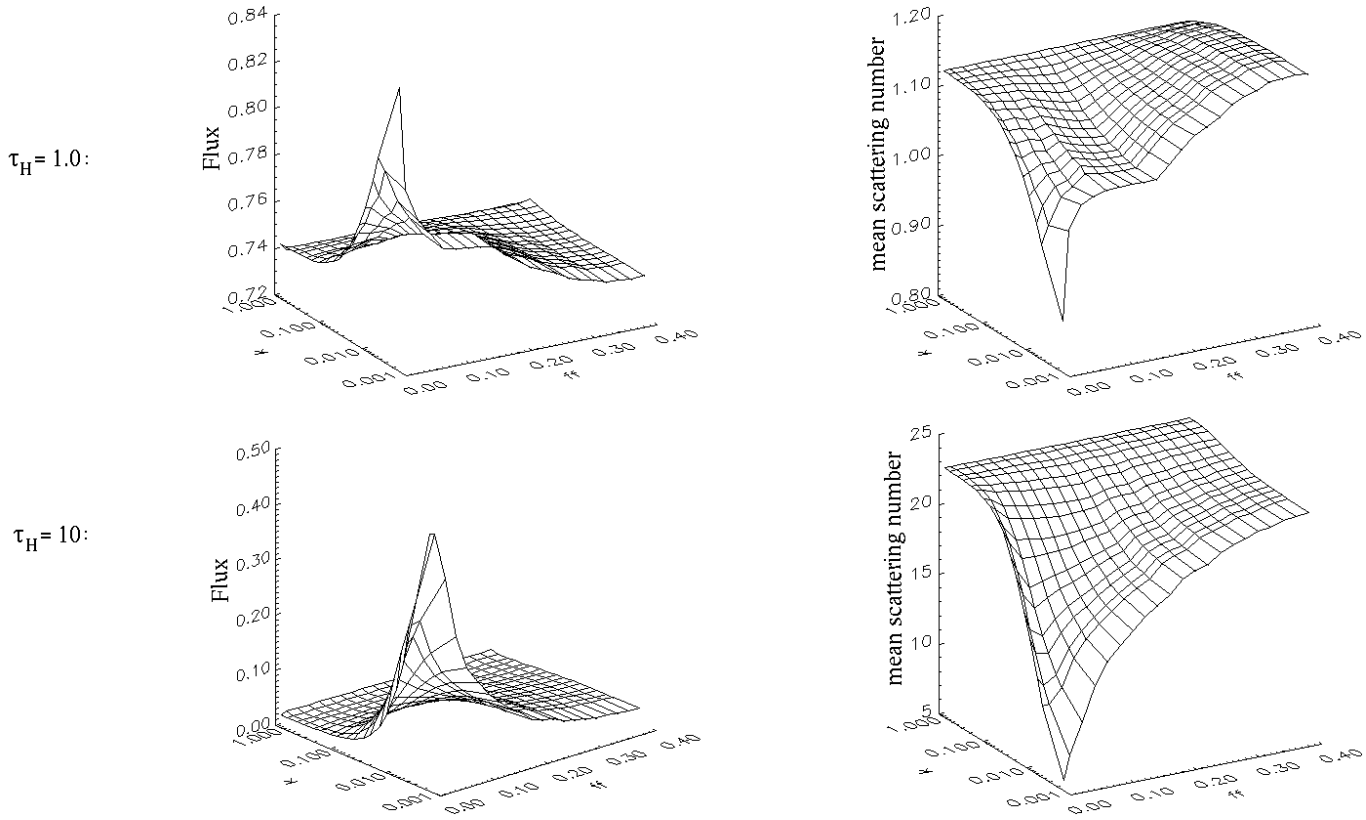

Fig. 16. Stellar flux outside the clumpy shell normalized to the stellar flux outside the equivalent homogeneous shell. Population G, λ = 550 nm.

connection between the smallest clump size and the observable stellar flux for the chosen filling factor and density ratio (k=0.01, ff=0.05). For shells with a "weak clumpiness" ($ff \to 1, k \to 1$), this deviation may not be neglected, because the difference between the stellar flux outside an homogeneous and a clumpy shell converges to zero. For the mean scattering number the same conclusion is valid.

3.2. Influence on the polarization of the stellar light

Matsumura & Seki (1995) found that the variation of the flux of the reflection nebula around R Mon is correlated with the degree of the linear polarization of the scattered light. They supposed that optically thick dust clouds cross the observers line of sight to the central star. By this, the direct unpolarized stellar radiation is attenuated and the nett polarization from the scattered, polarized radiation increases.

In contrast to this time-dependent effect, we investigated static systems. Our results represent time-averaged values. We started our modelling with $\tau_{\rm H} = 1$ at λ = 550 nm. The radial distribution of the degree of linear polarization $P_{\rm l}(r)$ is shown in Fig. 18, where r is the distance from the star projected on the polarization map. Three radius regions of interest are obvious in Fig. 19(A):

1. $\frac{r}{R_{\rm S}} < 30\%$: $P_{\rm l,ClumpyShell} < P_{\rm l,HomogeneousShell}$, reduction of the degree of polarization towards the star
   – The "unpolarized" photons started from the star have their first scattering more distant from the star in the clumpy shell.
2. $30\% \leq \frac{r}{R_{\rm S}} \leq 80\%$: $P_{\rm l,ClumpyShell} \geq P_{\rm l,HomogeneousShell}$
   – The first scattering of the test-photons occurs mainly in this radius region. As the single scattered photons contribute substantially to the observable polarization degree, the polarization is higher than in the case of an homogeneous shell, where the first scattering happens more close to the star. However, the degree of linear polarization increases noticeable only for $k < 0.01$ ($\frac{P_{\rm l}(k,r)-P_{\rm l}(k=1,r)}{P_{\rm l}(k=1,r)} \gg 1\%$). This result is in agreement with the behaviour of the stellar flux (see Sect. 3.1).
3. $\frac{r}{R_{\rm S}} > 80\%$: With increasing distance from the star, the degree of the linear polarization approaches for its corresponding value of the equivalent homogeneous shell.
   – Corresponding to $\tau_{\rm H}$, the n-th scattering ($n > 1$) dominates in this radius region. Photons which were scattered many times do not significantly contribute to the observable degree of linear polarization. The influence of the single scattered photons decreases with increasing distance from the star and approaches the corresponding value of the equivalent homogeneous shell.

The change of the radial distribution of $P_{\rm l}$ is mainly attributed to the shift of the radial distribution of the first scattering

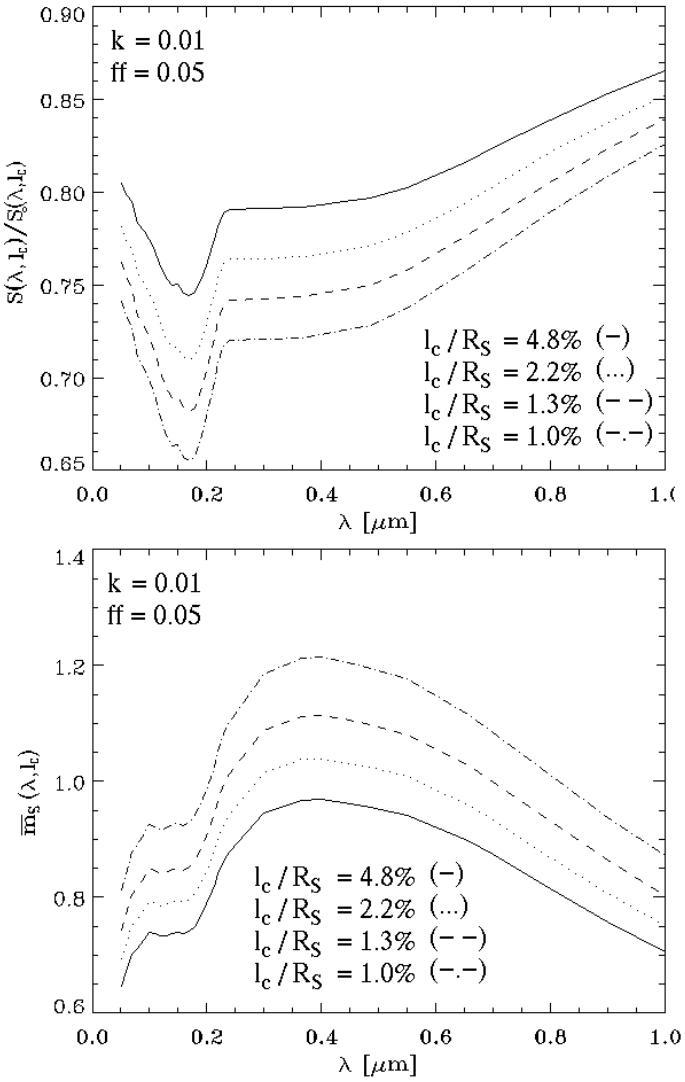

Fig. 17. Ratio of the integrated stellar flux outside a clumpy dust shell $S(\lambda, l_c)$ to the unattenuated stellar flux $S_0(\lambda, l_c)$ and the mean scattering number $\bar{m}_s(\lambda, l_c)$ for different grid sizes. $k = 0.01$, $ff = 0.05$. Population G

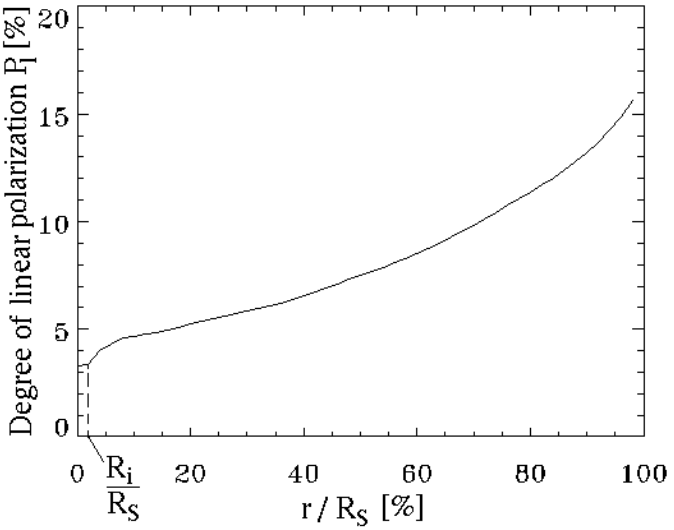

Fig. 18. Radial distribution of the degree of linear polarization P_l for an homogeneous shell. τ_H=1. r is the projected distance from the central star. Population K, λ = 550 nm, $\tau_H = 1$, Radius of the dust free region around the star: $R_i = 2.5\% R_S$

region towards larger radii. This is confirmed by the distributions shown in Fig. 20.

The character of the three mentioned radius regions depends on the optical depth, ff and k. For similar optical depths, the qualitative behaviour of the polarization degree was found to be wavelength independend. A low optical depth τ_H guarantees a low polarization in the first region because of the large mean free path length of the test-photons. In addition, the boundaries of the 2nd and the 3rd region are shifted outward.

The influence of ff (k=const.) can be interpreted in the same way (see Fig. 19(B)).

The relative change of the polarization degree due to the clumps does not change the qualitative shape of the radial distribution $P_l(r)$ significantly. The alignment of the polarization vectors (centro-symmetric polarization pattern) is not changed. However, in general the influence of clumps on the polarization of arbitrary circumstellar dust configurations cannot be neglected. As an example, we simulated the polarization pattern of the configuration shown in Fig. 21A. In contrast to the previously investigated fractal-like clump structures, we used an ideal structure consisting of two optically thick small spheres (2,3) embedded in an optically thin large sphere (1). The disturbance of the centro-symmetric dust distributions results in a disturbance of the centro-symmetric polarization pattern. Whereas both clumps are visible in the intensity map (Fig. 21B), the effect of the deeper embedded clump on the polarization pattern can be neglected (Fig. 21C).

3.3. Surface brightness distribution

In contrast to an homogeneous spherical dust shell, the radial surface brightness distribution of a clumpy shell depends on the observer position. For the comparison with homogeneous shells we deduced the average radial surface brightness distribution in a clumpy shell from radiative transfer simulations in several models, characterized by the same parameters, and always from a large number of observers positions, uniformly distributed over the full solid angle. The flux $S_{OB}(r_i)$ outside the clumpy dust shell, which symbolizes the radial surface brightness distribution, was determined at 50 different, equidistant projected radii ($r_{i+1} - r_i = \Delta r$) inside an aperture with an area of $\Delta r \times \Delta r$ in the observation plane. It was calculated depending on k and ff for both an optically thin shell ($\tau_H = 1$) and an optically thick shell ($\tau_H = 10$) - see Fig. 22. The received fluxes were normalized to $\sum_i S_{OB}(r_i, k = 1) = 1$ (varying k) respectively $\sum_i S_{OB}(r_i, ff = 0.4) = 1$ (varying ff).

For both cases, the surface brightness remarkably increases near the star ($\frac{r}{R_S} \leq 10\%$). This can be explained by the shortest photon paths close to the map centre and by the scattering characteristics.

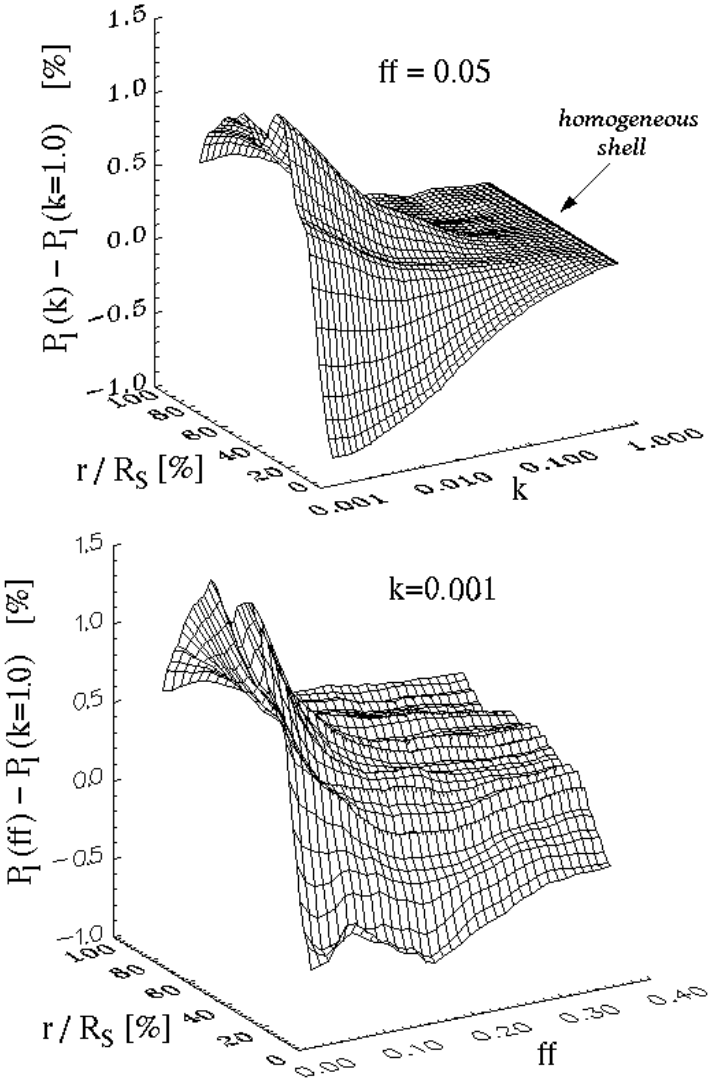

Fig. 19. Difference between the degree of linear polarization of the clumpy dust shell $P_{\rm l}(k, ff, r)$ and the polarization of the equivalent homogeneous shell $P_{\rm l}(k = 1, ff, r)$. r is the projected distance from the central star.

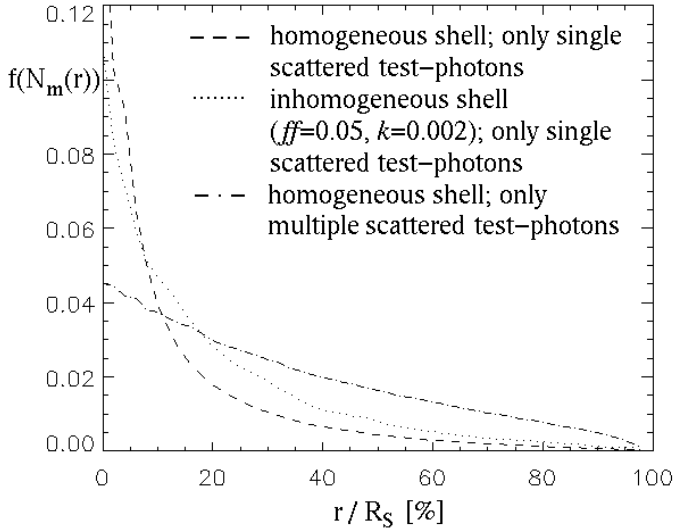

Fig. 20. Radial distribution of the last positions of scattering. The previous scattering parameters were used. r is the space distance from the star.

$N_{\rm m}(r)$ ... number of photons with the last scattering position in the distance r from the star

$f(N_{\rm m}(r))$ ... (normalized) distribution of $N_{\rm m}(r)$ ($\int_0^{R_S} f(N_{\rm m}(r))dr = 1$)

The radial surface brightness distribution as a function of ff and k depends on the optical depth $\tau_{\rm H}$ of the equivalent homogeneous dust shell.This effect can be explained by the appearance of two contrary tendencies. Decreasing the effective optical depth (decreasing the filling factor or the density ratio) the mean scattering number respectively the scattering probability decreases. This has two consequences:

1. At a given distance from the star the intensity of the observed test-photons is larger than for the equivalent homogeneous shell. This leads to an increasing surface brightness of the whole shell (see Fig. 22(C): $S_{\rm OB}(r, k \geq 0.005, ff = 0.05, \tau_{\rm H} = 10)$ and Fig. 22(D): $S_{\rm OB}(r, k = 0.01, ff \geq 0.04, \tau_{\rm H} = 10)$).
2. If the effective optical depth $\tau_{\rm eff}$ drops below a certain limit $\tau_{\rm GW}$, the total number of scatterings decreases and the shell is irradiated less effective. This leads to a decrease of the surface brightness beginning in the innermost parts of the shell (see Fig. 22(A); Fig. 22(B); Fig. 22(C): $S_{\rm OB}(r, k < 0.005, ff = 0.05, \tau_{\rm H} = 10)$; Fig. 22(D): $S_{\rm OB}(r, k = 0.01, ff < 0.04, \tau_{\rm H} = 10)$). If the positions of the first scattering shift to larger radii, the regions with reduced surface brightness shift outwards, too. Even if the number of single scattered photons, received from the shell increases, the surface brightness is negligible. This is caused by the fact that an optically thin shell is much brighter than an optically thick shell, even in the case of an homogeneous dust density distribution. The limit of the effective optical depth was determined to $\tau_{\rm GW} = 2.9 \pm 0.4$ using the considered models with $\tau_{\rm H} = 10$.

The observable flux from the innermost regions around the star ($\frac{r}{R_S} \leq 10\%$) drops about a factor of 3.1 ($\tau_{\rm H} = 1$; Fig. 22(B)) respectively 2.0 ($\tau_{\rm H} = 10$; Fig. 22(D)) at $ff \approx 0.20$ - only a few percent below the percolation threshold. Just like the second tendency, described above, this is caused by the effect, that the positions of the first scattering shift outwards and the illumination of the innermost region decreases. Increasing $\tau_{\rm H}$, this effect weakens.

Changing the K population dust by that of the G population, the behaviour of the surface brightness is similar, but less pronounced.

The investigation of optical very thin dust shells ($\tau_{\rm H} \ll 1$), where in the equivalent homogeneous shell the test-photons are scattered extremely seldom, shows that the appearance of clumpy structures increases the surface brightness of the shell. This is explained by the increased scattering probability of the "lighted up" clumps. This is especially important for long wave-

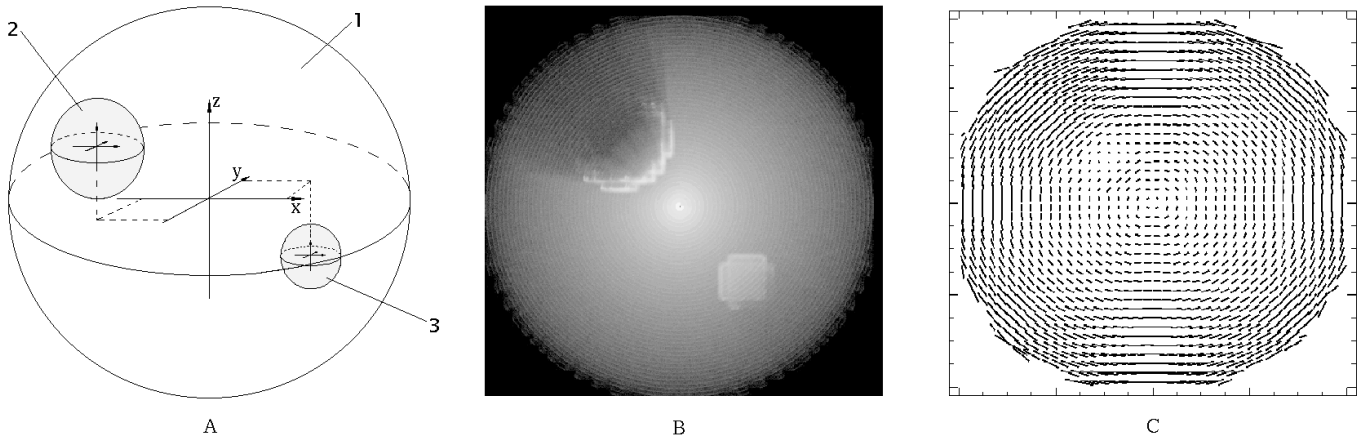

Fig. 21A–C. Model: "Big clumps". **A** Example for the influence of large spherical, optical thick clumps embedded in an optical thin medium on the polarization pattern of the shell. **B** Intensity map of the dust configuration shown in **A**. The observer looks along the positive y-axes. The discretization of the clumps is visible. **C** Polarization map of the dust configuration shown in **A**. The observer looks towards the y-axes. Model: τ(spherical shell -without clumps-)=0.2, τ(clumps)=100, $\lambda = 1.25\mu$ m, $N_{\rm x} \times N_{\rm y} \times N_{\rm z}$ = 46×46×46 grid points

length radiation. Visually observed reflection nebulae ($\tau_{\rm V} \leq 1$) are nearly transparent in the IR. Clumps may increase their IR surface brightness by the effect described above. The increased scattering probability becomes strong for UV-photons which heat the clumps. The absorbed energy is reradiated at IR wavelengths, what remarkably increases the surface brightness.

4. Conclusions

We treated the radiative transfer in a two-phase clumpy dust sphere for $\lambda = 0.050 \ldots 1.000\ \mu$m. Firstly, we showed the ability to describe real clumpy structures on the basis of our model. The modelled clumpy structures show a similar potential law of the clump and mass size distribution as being observed in the interstellar matter. Furthermore, in preparation of the radiative transfer simulations, we introduced the model parameters characterising 2-phase clumpy systems: the filling factor ff, the density ratio k and the effective optical depth $\tau_{\rm eff}$ as well as the optical depth for the equivalent homogeneous envelope $\tau_{\rm H}$. While $\tau_{\rm eff}$ is a significant indicator for the optical behaviour of clumpy envelopes, the influence of clumpiness on the radiative transfer can be deduced from the distribution of the optical depth $P(\tau)$ as well.

It has been shown that the quantitative behaviour of the radiative transfer can be derived from $\tau_{\rm eff}$ as a function of ff, k and $\tau_{\rm H}$. By this way, it is possible to decide, in which cases the radiative transfer in clumpy spherical dust shells can be treated like in homogeneous shells, and in which cases the radiative transfer calculations on the basis of homogeneous models would lead to significant differences.

In the second part of the paper we investigated the behaviour of the radiative transfer due to the changes of the different model parameters. In agreement with the results of the first part of this paper we found that the qualitative behaviour of the investigated radiative transfer parameters can mainly be derived from the influence of changing model parameters on the effective optical depth. The radiative transfer in a clumpy dust shell differs significantly from that in the equivalent homogeneous shell, if both the filling factor and the density ratio simultaneously fall below "critical values". These "critical values" are functions of the equivalent optical depth.

We introduced the radial rate of absorption AR, which is proportional to the amount of energy which has been stored at a certain distance from the star due to absorption. In the case of the stellar radiation it indicates the regions, where the transfer from UV/visible to IR/FIR radiation takes place. For the inter-clump medium we found a decrease of the gradient of AR for decreased filling factors and density ratios. The consequence is a temperature decrease which is more flat in a clumpy envelope.

In agreement with Natta & Panagia (1984) we found that the short wavelength radiation is modified by nearly grey extinction if the optical depth of the clumps is sufficiently high and that of the inter-clump medium is sufficiently low. This leads to weakened absorption bands.

The smallest clump size, given by the dimension of a single cube, has found to be an additional basic parameter of our model. Treating the radiative transfer in clumpy systems with a density structure defined corresponding to the description in Sect. 2, one has always to test, whether there exists a lower clump size threshold value, or not. In the case of our model, there is no difference between a clumpy and an homogeneous stellar envelope if the smallest clump size converges to the mean distance between the dust particles. The threshold value has to be derived from the process, which is responsible for the occurrence of the clumpy structure.

The qualitative shape of the polarization pattern changes only insignificantly due to occurrence of clumpy structures. In difference to this, the quantitative behaviour of the radial polarization distribution depends on the filling factor, the density ratio and the (effective) optical depth. But, the estimated differences between a clumpy and an homogeneous shell are always rather small.

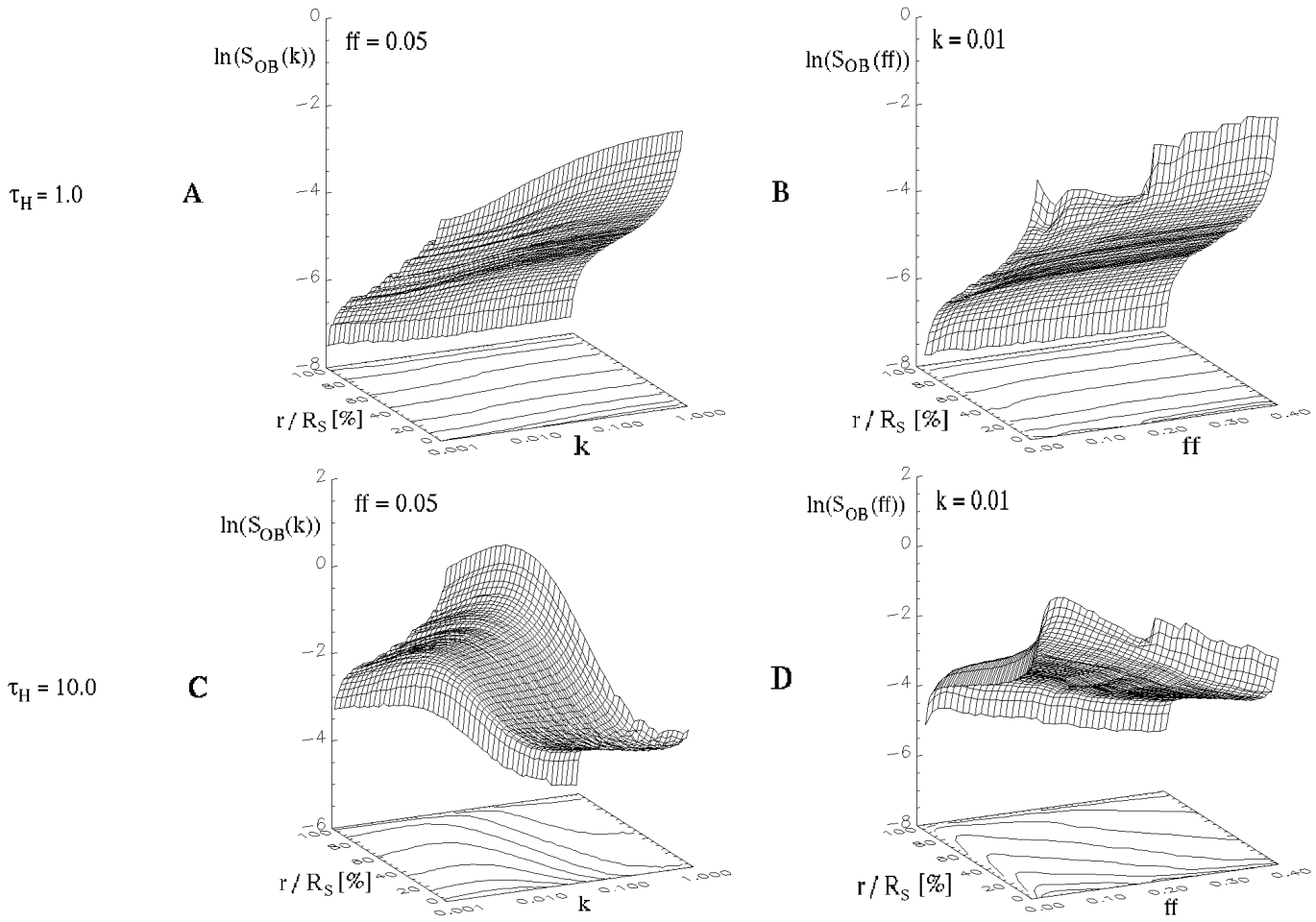

Fig. 22. Surface brightness $S_{\rm OB}(r, k, ff, \tau)$. K-Population, λ = 550 nm

Consistent with results from Witt & Gordon (1996), we found the qualitative behaviour of the surface brightness distribution to be fundamentally dependent on the optical depth of the equivalent homogeneous shell $\tau_{\rm H}$.

Future attempts of the treatment of radiative transfer in clumpy systems should direct attention onto special clump structures.

References

Boissé P., 1990, A&A 228, 483

Burton M. G., D.J. Hollenbach D. J., Tielens A. G. G. M., 1990, ApJ 365, 620

Capetti A., Axon D. J., Macchetto F., Sparks W. B., Boksenberg A., 1995a, ApJ 446, 155

Capetti A., Macchetto F., Axon D. J., Sparks W. B., Boksenberg A., 1995b, ApJ 448,600

Capetti A., Macchetto F., Axon D. J., Sparks W. B., Boksenberg A., 1995c, ApJ 452, L87

Chen W., Naya J., Gehrels N., Tueller J., Hartmann D., 1996, BAAS 189, 117.01

Colomb F. R., Pöppel W. G. L., Heiles C., 1980, A&AS 40, 47

Dickey J. M., Garwood R. W., 1989, ApJ 341, 201

Draine B. T., Lee H. M., 1984, ApJ 285, 89

Falgarone E., Phillips T.G., Walker C. K., 1991, ApJ 378, 186

Fischer O., Henning Th., Yorke H. W., 1994, A&A 284, 187

Frisch, P.C., 1996, BAAS 188, 44.08

Grinin V. P., Thé P. S., de Winter D., Giampapa M. S., Rostopchina A. N., Tambovtseva L. V., van den Ancer M., 1994, A&A 292, 165

Grinin V. P., Kozlova O., Thé P. S., Rostopchina A. N., 1995, A&A 309, 474

Grinin V. P., Natta A., Tambovtseva L. V., 1996, A&A 313, 857

Herbstmeier U., Moritz P., Engelmann J., Kerp J., Westphalen G., 1993, Proc. of the 3rd ann. Astrophys. Conf. in Maryland “Back to the Galaxy”

Hobson M. P., Padman R., 1993, RASMN 264, 161

Hobson M. P., Scheuer P. A. G., 1993, RASMN 264, 145

Kishimoto M., 1997, Ap&SS 184, 277

Macchetto F., Capetti A., Sparks W. B., Axon D. J., Boksenberg A., 1994, ApJ 435, L15

Lagrange A-M., Ferlet R., Vidal-Madjar A., 1987, A&A173, 289

Matsumura M., Seki M., 1995, ApSS 24, 513

Meixner M., Tielens A. G. G. M., 1993, ApJ 405, 216

Meixner M., Tielens A. G. G. M., 1995, ApJ 446, 907

Meyer D. M., Blades J. C., 1995, BAAS 187, 45.04

Mitskevich A. S., 1994, A&A 281, 471

Mitskevich A. S., 1995, A&A 298, 231

Natta A., Panagia N., 1984, ApJ 287, 228

Rohlfs K., Luks T., 1992, New Aspects of Magellanic Cloud research, European meeting on the Magellanic Cloud, 2nd, SFB No. 328 'Evolution of Galaxies', A95-88790, p. 115
Rosen A., Bregman J. N., 1995, ApJ 440, 634
Spaans M., 1996, A&A 307, 271
Spyromilio J., Malin D. F., Allen D. A., Steer C. J., Couch W. J., 1996, MNRAS 274, Issue 1, 256
Stauffer D., Aharony A., Perkolationstheorie, VCH Verlagsgesellschaft mbH, 1995
Stacey G. J., 1993, ApJ 404, 219
Witt A., Gordon K. D., 1996, ApJ 463, 681
Young L.M., 1996, BAAS 189, 84.01